Quantifying speckle noise in Shack-Hartmann wavefront sensing

Gregory W. Allan
Massachusetts Institute of Technology, Cambridge, MA, USA

Lulu Liu
MIT Lincoln Laboratory, Lexington, MA, USA

Kerri Cahoy
Massachusetts Institute of Technology, Cambridge, MA, USA

ABSTRACT

Adaptive optical compensation for imaging or illumination of a remote object relies on accurate sensing of atmospheric aberrations. In the case of a laser system for engagement of space debris, the reflected light from the target can be used as an artificial guide-star for wavefront sensing. Sensing with reflected light is desirable because it is sensitive to tip-tilt aberrations and is not subject to focal anisoplanatism, unlike sensing with laser guide-stars. However, the coherent illumination of a target object with surface roughness on the scale of a wavelength results in random interference in the reflected wave, and ultimately in speckling of phase and amplitude in the far field. In a Shack-Hartmann Wavefront Sensor (SHWFS) measurement, these speckles cause fluctuations in the intensity of focal spots and errors in the position of their centroids relative to those expected from purely atmospheric effects. The resulting wavefront measurements therefore cannot be used for accurate atmospheric phase conjugation. This paper discusses the effect of reflected laser speckle on the accuracy of SHWFS measurements. We provide experimental validation that averaging of SHWFS lenslet spot intensities over speckle realizations converges to the incoherent intensity as expected. We show via simulation that the speckle-induced error in centroiding is a function of the ratio between target size and the diffraction limited resolution of the lenslet. We further show that the effects of shot noise and speckle noise add in quadrature, allowing simple noise analysis. This work provides a straightforward set of relations which can help investigators more accurately estimate the required integration time for a target-in-the-loop wavefront sensing system.

1. INTRODUCTION

The ability to project light with high power and directivity from the ground into space has many applications. In the near-term, proposed projects include orbit modification or removal of debris in low earth orbit (LEO) [1], and deep-space optical communications (DSOC) [2], while further in the future advances in laser technology and distributed arrays will enable laser propulsion of spacecraft [3] and deflection of potentially dangerous near-earth objects [4]. This paper focuses in particular on the space debris application.

To focus a beam on a small object at orbital ranges, a large aperture is needed ($D > 5\,\mathrm{m}$ for a 10 cm spot in LEO in the near-IR). Apertures of this size require adaptive optics to correct for atmospheric aberrations and a source of light for use as a guide-star. If a suitable natural guide-star is not nearby, an artificial laser guide-star can be used. However, the wavefront generated by a sodium guide-star originates at an altitude of 90 km, and so the cone effect (focal anisoplanatism) causes error in wavefront correction. These errors limit the use of a single laser guide-star to apertures of less than 10 m in diameter, even in the best atmospheric conditions [5]. The outgoing laser guide-star light is also affected by atmospheric turbulence, so the apparent position of the sodium beacon cannot be used for atmospheric tip-tilt correction.

If the beacon light instead originates at the target, these effects are not present. In the case of an uncooperative target such as orbital debris, natural illumination conditions may not be sufficient to achieve the signal-to-noise ratio (SNR) required for wavefront sensing. If instead enough light from the beam director is able to reach the target, the scattered light could be used as a beacon. However, illumination of a rough target with a coherent beam causes laser speckle in the reflected light. In an adaptive optics system, the random phase and amplitude fluctuations due to speckle presents a confounding signal for wavefront sensing necessary to perform atmospheric phase conjugation. For a Shack-Hartmann Wavefront Sensor (SHWFS) specifically, the phase and intensity fluctuations due to speckle cause the spots formed by each lenslet to be speckled. That is, the spot intensity has random variations compared to an image of the same object under incoherent illumination. The operation of a SHWFS relies on an algorithm to obtain the centroid of the image to determine the local wavefront slope. In the presence

Copyright © 2020 Advanced Maui Optical and Space Surveillance Technologies Conference (AMOS) – www.amostech.com

of speckle, the slope measurements reflect the properties of the speckle field, rather than that of a true atmospheric measurement.

Methods for suppressing the effects of optical speckle rely on incoherent addition of speckle realizations through diversity of angle, wavelength, polarization, or other properties [6]. One proposed method for object-based sensing uses varying illumination and observation angle to independently measure the wavefront contributions from atmosphere, instrument, and speckle [7]. However, varying illumination angle is not practical when constant illumination of the target through a dynamic atmosphere is required. More common in object-based wavefront sensing applications is the averaging of speckle by using the natural rotational motion of the target to present many surface roughness realizations. When target motion is not enough, averaging can be performed by scanning of the illumination spot across the object. If the surface of the target object is assumed to be rough on the scale of a wavelength, target-induced phase can be ignored and the speckle-average wavefront slopes are an unbiased measurement of the atmospheric phase [8]. Speckle averaging has been shown to improve sensing of aberrations in the human eye [9], and to improve atmospheric wavefront correction performance in a target-in-the-loop (TIL) system [10]. However, with any amount of averaging there will always be a residual speckle effect. When the target is small and slowly rotating, these averaging methods may not reduce the level of this error to below that of the usual error sources such as photon noise. It is therefore important to quantify the speckle error for design of target-in-the-loop beam projection systems.

To date, the error due to speckle in a SHWFS has been studied empirically for low order Zernike aberration terms in the context of the human eye [11, 12]. A key result is an inverse relationship between root-mean-square (RMS) wavefront error and the quantity D_{corr}/D_{ap}, where D_{corr} is the speckle correlation length and D_{ap} is the diameter of the SHWFS lenslets. These works provide some insight into the physical phenomena underlying the measurement accuracy, but do not provide a concise physical relationship between the parameters of the optical system and resulting measurement error. Such a relationship is crucial for performance analysis of large-scale beam projection systems.

The objective of this paper is to establish clear criteria to obtain diffraction-limited performance for a beam director (or imaging system) using a Shack-Hartmann wavefront sensor with a coherently-illuminated target. The analysis focuses on centroiding error due to the random speckle field, referred to here as *speckle noise*, and on the interaction and relative contributions of speckle noise and photon noise across a wide range of illumination intensities and target and sensor scales.

2. THEORY

The use of a SHWFS depends on the localization of the centroid of the focal spot formed by the lenslet. The angular displacement of the focal spot coincides with the average wavefront tilt over the aperture [13]. There are many methods of estimating the centroid, including simple center-of-mass (CoM), thresholded, weighted, and windowed CoM, matched filtering, and others. Here we focus on the simple CoM method, whose centroiding operators in the x and y directions are defined by

$$c_x = \frac{\sum_{i,j} x_{i,j} H_{i,j}}{\sum_{i,j} H_{i,j}} \quad \text{and} \quad c_y = \frac{\sum_{i,j} y_{i,j} H_{i,j}}{\sum_{i,j} H_{i,j}}. \tag{1}$$

Where $H_{i,j}$ is the measured intensity in a pixel in photons, and $x_{i,j}$ or $y_{i,j}$ is the location of that pixel in angular units. All further analysis will be done along the x direction, with no loss of generality. The variance in centroid angular location will be designated $\sigma_\alpha^2 = \mathrm{Var}(c_x)$, and is given by

$$\sigma_\alpha^2 = \frac{1}{N_{ph}^2} \sum_{i,j} \sum_{k,l} x_{i,j} x_{k,l} \mathrm{Cov}(H_{i,j}, H_{k,l}). \tag{2}$$

Where N_{ph} is the total intensity or number of photons per frame with $\sum_{i,j} H_{i,j} = N_{ph}$. The variance can be derived from Eq. 1 with the assumption that total intensity does not change appreciably due to speckle or scintillation effects [14]. The term $\mathrm{Cov}(H_{i,j}, H_{k,l})$ depends on random variation due to both the random speckle and Poisson noise, where Poisson noise is itself a function of the speckle intensity in a given frame. Despite this compound noise relationship, the total centroid variance can be represented as a sum of two independent terms, corresponding to photon noise and speckle noise.

$$\mathrm{Cov}(H_{i,j}, H_{k,l}) = \mathrm{Cov}_{ph}(H_{i,j}, H_{k,l}) + \mathrm{Cov}_{spk}(H_{i,j}, H_{k,l}) \tag{3}$$

$$\sigma_\alpha^2 = \sigma_{ph}^2 + \sigma_{spk}^2 \tag{4}$$

Copyright © 2020 Advanced Maui Optical and Space Surveillance Technologies Conference (AMOS) – www.amostech.com

This property greatly simplifies analysis, and is derived in App. A. The forms of these two error terms are discussed in Sec. 2.1 and 2.2. The exact value of σ_{spk}^2 is difficult to determine through analytical means and is the subject of Sec. 3 and 4.

The most relevant metric when analyzing system performance is not just centroiding precision, but accuracy of the overall wavefront reconstruction. The reconstruction error, assuming uncorrelated slope measurement noise, is proportional to the error in measured phase difference across the SHWFS lenslet apertures, as

$$\sigma_\phi = 2\pi G_e \frac{D_{ap}}{\lambda} \sigma_\alpha. \tag{5}$$

Where σ_ϕ is the RMS error in the wavefront reconstruction, and D_{ap} is the diameter of each lenslet aperture. The value of the error propagation parameter G_e depends on the sampling geometry of the SHWFS sensor, and tends to increase with increasing number of SHWFS subapertures. Some values for this parameter are given by [15], assuming uncorrelated errors between subapertures. In this work we take $G_e = 1$ as a limiting case for a large number of subapertures (> 20) in Southwell's reconstruction geometry (measurement and reconstruction points co-located).

2.1. Photon Noise

The portion of the centroiding error variance due to photon noise is given [16] by

$$\sigma_{ph}^2 = \frac{1}{N_{ph}^2} \sum_{i,j} x_{i,j}^2 \langle H_{i,j} \rangle. \tag{6}$$

Here, we take $\langle H_{i,j} \rangle$ as a shorthand for the speckle-mean intensity of the target image at coordinates $(x_{i,j}, y_{i,j})$, or the image for an incoherently illuminated target. This calculation depends on the size and shape of the target and the parameters of the imaging system. In the general case, we note that the intensity is the convolution of the target object intensity and the point-spread function of the lenslet aperture. Since the centroid variance is simply the second moment of the intensity distribution, it can be calculated as the sum of the second moments of its two component distributions. Therefore

$$\sigma_{ph}^2 = \sigma_{circ}^2 + \sigma_{diff}^2. \tag{7}$$

For the case where the target is well resolved, a circular top-hat intensity profile is assumed, with centroiding error

$$\sigma_{circ}^2 = \frac{1}{16 N_{ph}} \theta_{targ}^2. \tag{8}$$

A derivation of Eq. 8 is provided in App. B. In the case where the target is unresolved, the intensity profile approaches an Airy disk, with centroiding error which can be approximated using the diffraction pattern for a square aperture [16]

$$\sigma_{diff}^2 = \frac{w}{2\pi^2 N_{ph}}. \tag{9}$$

We notice that the error grows as the angular size w of the sensor field of view (FOV), since more diffraction rings are always visible with increasing FOV.

2.2. Speckle Noise

A rough target of size D_{targ}, illuminated with coherent light, will reflect a speckle pattern into the far field. The surface roughness of the object determines the overall scattering angle of the reflected light. The shape of the autocovariance function of the complex field depends on the overall shape of the object, but has a width which can be defined [6] as

$$D_{corr} = \frac{2\lambda z}{\sqrt{\pi} D_{targ}}. \tag{10}$$

Where D_{corr} refers to the square root of the speckle intensity correlation area, and z is the range to the target. An object that is well resolved by an aperture of size D_{ap} (so $D_{targ} >> \lambda z / D_{ap}$) therefore creates speckles much smaller than the aperture, while unresolved objects result in correlation lengths much larger than the aperture. The behavior of the focal plane in these limits differs greatly, and so a key parameter in the analysis is the ratio of the angular extent of the target to the angular width of the diffraction spot formed by the aperture, given by

$$\zeta = \frac{\theta_{targ}}{\theta_{diff}} = \frac{D_{targ} D_{ap}}{\lambda z}. \tag{11}$$

Copyright © 2020 Advanced Maui Optical and Space Surveillance Technologies Conference (AMOS) – www.amostech.com

We note that this quantity is inversely proportional to D_{corr}/D_{ap}. The analysis that follows is intended to be applicable over many orders of magnitude ($10^{-3} < \zeta < 10^{2}$). We further assume that the target is uniformly illuminated and circular in shape, imaged through a circular lenslet aperture.

As shown in App. C, σ_{spk} is expected to be proportional to ζ for unresolved targets. For resolved targets, the speckle covariance term in Eq. 3 is expected not to change with ζ, because the correlation function of the speckle is set by the diffraction limit of the aperture as the speckles become finer than that limit [6]. We note that unlike with photon noise, an increase in the size of the target does not result in increased error. We therefore perform a fit to the simulation data using a function of the form

$$\sigma^2_{spk,0} = \left(\frac{a\zeta}{b+\zeta}\right)^2. \tag{12}$$

Where $\sigma^2_{spk,0}$ is the mean-squared-error (MSE) of the centroid for instantaneous measurements.

We must also address the effect of finite instrument integration time on σ^2_{spk}. Averaging the effect of many independent speckle realizations reduces the effect of optical speckle. The simplest case to analyze is that in which individual frames are averaged together, with each from being the result of a statistically independent, identically distributed speckle realization. In this case, the variance of the speckle noise decreases as the number M of independent realizations averaged.

$$(\sigma_{spk})^2 = \frac{1}{N_{spk}}\sigma^2_{spk,0} \tag{13}$$

This relationship is derived in App. D. Continuous time averaging of an evolving (translating) speckle field can be described in the same terms. If the field evolves over M independent speckle realizations, we can treat the average image plane intensity integrated over time as a speckle field with contrast C [6], where

$$C = \frac{1}{\sqrt{M}}. \tag{14}$$

Eq. 13 and 14 agree with the result in [9] that RMS wavefront error is proportional to speckle contrast. This property will be used in the analysis of system performance in Sec. 5.

3. METHOD

To determine the relationship of the speckle-induced centroiding noise σ_{spk} to the parameters of the SHWFS imaging system, a physical optics simulation was developed. An experimental validation of the simulation results was then attempted. The results of this effort are presented in Sec. 4.

3.1. Simulation

To simulate the imaging of a coherently-illuminated rough target we take the general approach of plane-to-plane propagation using the Fresnel approximation. We assume that the target is circular and uniformly illuminated (a reasonable assumption for initial illumination, before the beam director is tightly focused). The target is assumed to have a surface that is δ-correlated, such that each discretization point has a random phase drawn from a uniform distribution between 0 and 2π radians. The field at the target is first propagated to the ground/pupil plane, the pupil function is applied, and then the pupil field is propagated to the image plane.

Fresnel propagation is chosen, since for large target size, even orbital distances put the ground-based array in the target's near field. For example, the Fresnel number $D^2_{targ}/4\lambda z = 25$ for a target diameter $D_{targ} = 10\,\text{m}$, wavelength $\lambda = 1\,\mu\text{m}$ and range $z = 1000\,\text{km}$. The Fresnel propagation is computed via a Fourier transform of the field multiplied by the appropriate quadratic phase factor [17]. For the propagation from target to the ground, use of the conventional Fast Fourier Transform (FFT) algorithm would require excessive zero-padding in the target plane to achieve the necessary sampling in the pupil plane. Since the area of regard in the pupil plane is small compared to the maximum angular frequency content of the target field, the transform can efficiently be computed over a limited domain using a Matrix Direct Fourier Transform, as described in [18], drastically decreasing computation time for this geometry. The field in each of these three planes is shown in Fig. 1.

To estimate σ_{spk}, centroiding of the image-plane intensity was performed as in Eq. 1. System parameters for these simulations were chosen and varied as shown in Table 1. The ranges of each parameter were discretized into 10 logarithmically-spaced points, for 1000 total combinations. For each combination of these parameters, $N_{spk} = 5000$ independent speckle realizations were simulated, using a different random target phase pattern for each. The effects of photon noise and electronic sensor noise are not included.

Copyright © 2020 Advanced Maui Optical and Space Surveillance Technologies Conference (AMOS) – www.amostech.com

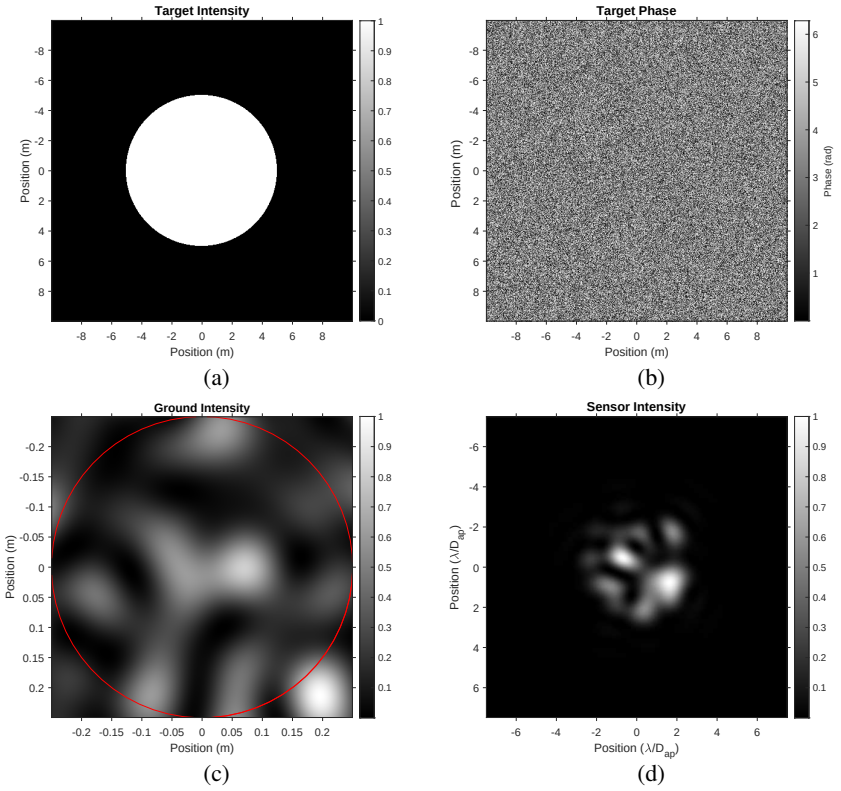

Figure 1: Example of plane-by-plane propagation of a simulated speckle realization. The field at the target plane is defined by the intensity (a) and a random δ-correlated phase realization (b). The field is propagated to the pupil plane using Fresnel diffraction (c), and the pupil function is applied (red solid line). The field in the aperture is then propagated to the image plane (c).

Parameter	Symbol	Values
Wavelength	λ	1 µm
Target Diameter	D_{targ}	10 cm to 100 m
Aperture Diameter	D_{ap}	5 cm to 5 m
Target Range	z	500 km to 5000 km
Norm. Angular Extent	ζ	10^{-3} to 10^{2}

Table 1: Parameters for simulation of target speckle propagation. Wavelength was held constant for all simulations. The resulting range of normalized angular target extent determined by combinations of the other parameters is also shown.

3.2. Experiment

In order to validate the assumptions and simulation results in this analysis, the imaging of a circular target with random phase was performed in the lab. As shown in Fig. 2, a $4f$ imaging system was set up with an adjustable pupil. The imaging target was a holographic diffuser behind a 100 µm pinhole. The diffuser was illuminated from behind by a 635 nm fiber-coupled, Fabry-Perot laser source. Independent speckle realizations were generated by rotating the diffuser to expose a different area through the pinhole. The system captures $N_{spk} = 135$ independent speckle realizations for each iris position. The iris was varied in size from $D = 5$ mm to $D = 15$ mm, so ζ varies from 1.0 to 3.1. The limitations of this experimental setup prevented measurement over a wider range.

4. RESULTS

4.1. Simulation

Error in the centroid position is reported in units of λ/D_{ap} (angular uncertainty). In terms of these units, the measurement error due to speckle is found to depend only on the parameter $\zeta = \theta_{targ}/\theta_{diff}$. These results are shown in Fig. 3. Though the error was simulated for many combinations of geometric parameters, the variance between experiments is small when plotted in the afforementioned coordinates. Furthermore, the mean is seen to

Copyright © 2020 Advanced Maui Optical and Space Surveillance Technologies Conference (AMOS) – www.amostech.com

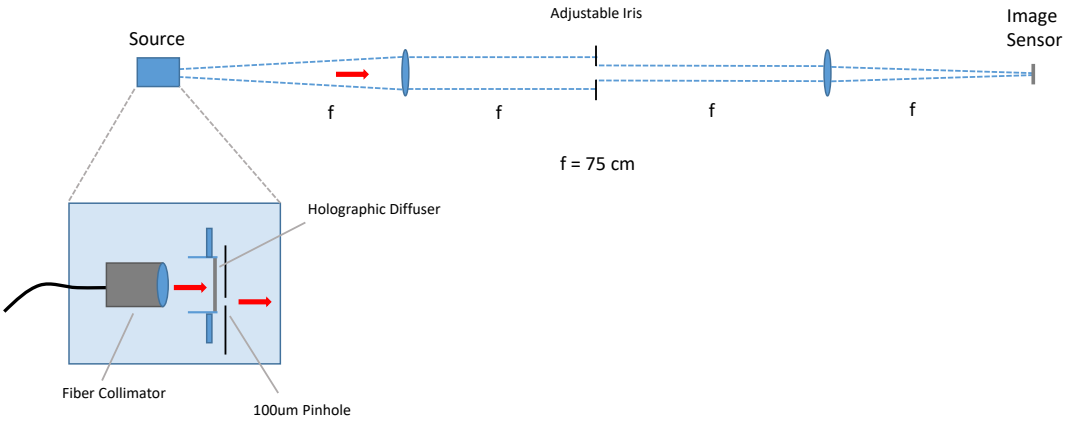

Figure 2: Laboratory setup to measure centroiding error due to laser speckle. Reflection from a rough target is simulated by illumination of a holographic diffuser followed by a pinhole using a 635 nm laser. Light from this object is imaged onto a sensor through an adjustable iris, used to vary the parameter $\zeta = \theta_{targ}/\theta_{diff}$. Arrows indicate direction of laser propagation.

be centered around zero, showing no bias in the centroids. A least-squares fit to the logarithmically re-expressed simulation data in Fig. 3a resulted in the coefficients $a = 0.279$, $b = 0.673$.

We note that the data in the RMS error curve appears to spread for lower values of ζ. Despite the variance θ_{spk} being reduced, the sample variance of the estimate grows. This can be explained by the statistics of phase slope in a speckle field. In the unresolved case $D_{corr} >> D_{ap}$, so the slope over the aperture is rougly constant and the measurement can be considered a true measurement of the speckle phase slope. The distribution of the slope of a speckle field has long tails and its true variance is indefinite, as shown in App. C.

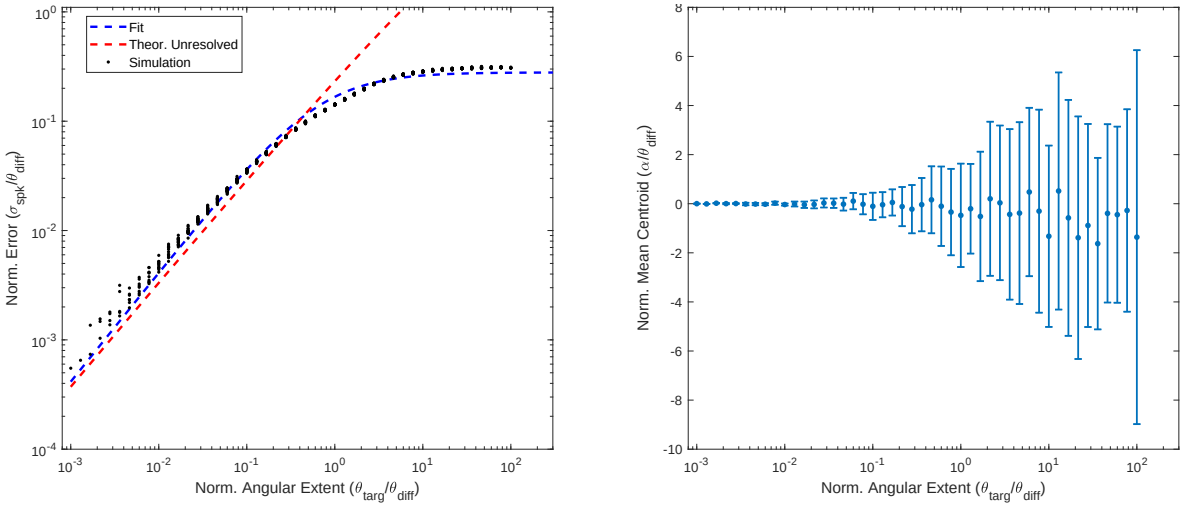

Figure 3: Simulated centroiding RMS error due to optical speckle effects (a), where each point corresponds to a combination of the varied geometric parmeters. Each point is the sample standard deviation of 5000 independent simulated speckle realizations. The theoretical curve for error in the unresolved case is as shown in App. C. A least squares fit for the parameters of Eq. 12 yielded $a = 0.279$, $b = 0.673$. (b) shows the mean value of centroid position for each value of normalized angular extent. Error bars show standard deviation of the mean centroid values for the different combinations of parameters that result in the same value of normalized angular extent.

4.2. Experiment

The captured images of each speckle realization and the average of all realizations illustrate that the average over many realizations is indeed a diffraction-limited spot. These results are shown in Fig. 4a. Note that as the aperture grows and the target becomes more resolved, more speckles are incident on the pupil plane and more speckle lobes are visible in the image.

Centroiding each of the images allows an estimate of the centroiding error due to speckle. The standard deviation of the measured centroids for each aperture diameter are plotted in Fig. 4b overlaying the simulated

Copyright © 2020 Advanced Maui Optical and Space Surveillance Technologies Conference (AMOS) – www.amostech.com

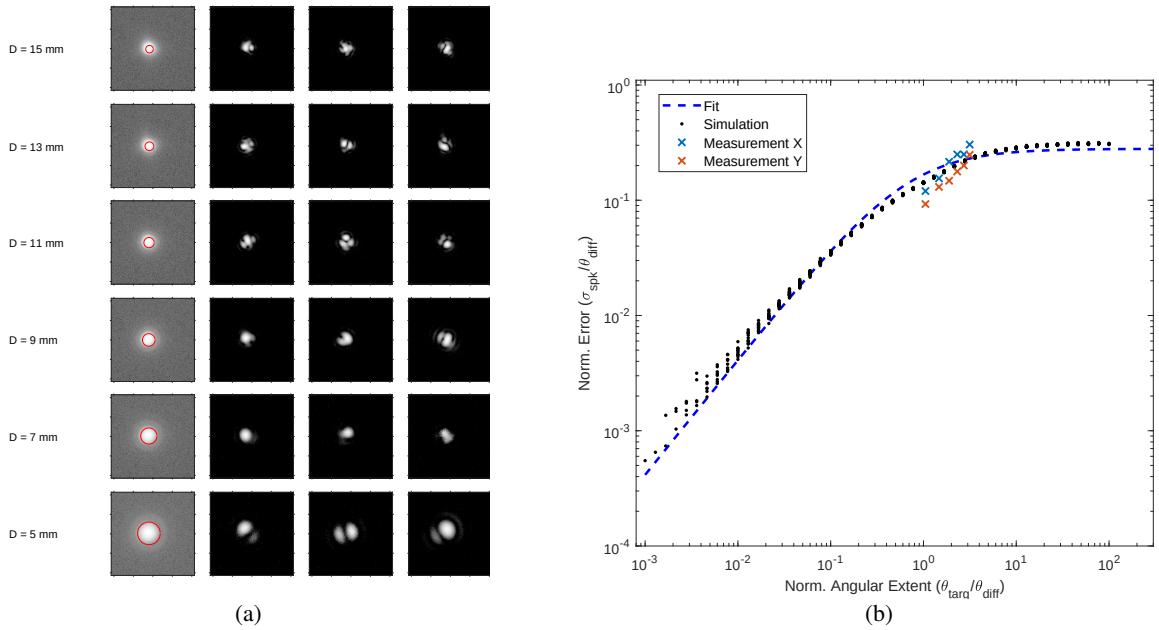

(a) (b)

Figure 4: (a) Laboratory measurement of speckle-averaged spot over 135 realizations shown for each tested aperture diameter (left-most column), and 3 example speckle realizations for each. The increase in fine structure of speckle for better-resolved targets can be seen. The red circle has a radius of $1.22\lambda/D$. (b) Experimental results for normalized RMS centroiding error for due to laser speckle for a single SHWFS subaperture, compared with simulated results. Estimated as the std. dev. of X and Y centroids of the images over many speckle iterations. Lab measurements agree qualitatively with the simulation, but over too narrow a range of ζ to verify the model.

data. There are two points for each aperture diameter as centroid error in x and y directions are shown for each. We see that the standard deviation measured from lab data agrees with the simulation, but the trend is not obvious. There is also an offset between X and Y centroid variance that points to a systematic error such as aberrations in the imaging system. It is is clear that a wider experimental range of $\theta_{targ}/\theta_{diff}$ is needed. An increase in the number of speckle realizations would also help to reduce the sample variance. An increase in integration time would help to rule out the effects of photon and readout noise. An improved experimental procedure will be the subject of future work.

5. DISCUSSION

Now that we have determined the basis for calculating photon and speckle noise, we can combine Eq. 7 and Eq. 12, to estimate the total noise variance in the presence of both speckle and photon noise. Combining with Eq. 5 we can determine the overall wavefront sensing performance. Furthermore, we can solve for required integration time to reach a given value of σ_ϕ. This allows us to determine the suitability of a wavefront sensing system to operate under given conditions.

To illustrate this analysis we use a scenario involving an attempted engagement of orbital debris by a beam director. We make the assumption that the shot noise SNR is determined by

$$N_{ph} = R_{ph}T. \tag{15}$$

Where R_{ph} is the optical power on the sensor in photons per second, and T is the integration time. The level of speckle noise is determined by

$$N_{spk} = R_{spk}T. \tag{16}$$

The the rate of speckle evolution R_{spk} depends on the motion of the target and the resulting evolution of the speckle field. In Fig. 5a, we provide a contour plot of the required integration time in seconds to reach a wavefront sensing MSE level of 1×10^{-3} rad^2. The values can be easily scaled to other error levels since the required time is inversely proportional to the error level required.

We can gain further insight about the dominant source of wavefront error under various conditions by treating the dynamic speckle field as a translating static field. We assume that the translation of the field is due to a rotation of the target object, and that the rate v of speckle translation is defined by $v = \omega z$ where ω is the target's apparent

Copyright © 2020 Advanced Maui Optical and Space Surveillance Technologies Conference (AMOS) – www.amostech.com

rotation rate. We also make the approximation that a speckle realization update occurs when the speckle field has translated by the aperture diameter, such that

$$R_{spk} = \frac{v}{D_{ap}}. \tag{17}$$

Note that Eq. 17 does not hold for $\zeta << 1$ where the speckle coherence length is much larger than the aperture. For this example, we assume that the target is at the zenith, at a range of 1000 km and moving at an associated orbital velocity of 7.36 km s^{-1}, resulting in an apparent angular velocity of $\omega = 7.36$ mrad s^{-1}. The diameter of the Shack-Hartmann subaperture is assumed to be 20 cm, with a FOV of $8\lambda/D_{ap}$. Results of this analysis are shown in Fig. 5b and 5c . We see that for high and low values of $\zeta = \theta_{targ}/\theta_{diff}$, the photon noise dominates, but in the region where the target is just resolved, the effect of speckle noise is evident. Even for this slowly-rotating target, integration times short enough to be accommodated by a 2000 Hz control loop bandwidth are sufficient to achieve low wavefront error. The value of R_{spk} under realistic conditions deserves further study, and is especially important for targets of sizes around the diffraction limit, where speckle error becomes dominant for bright targets.

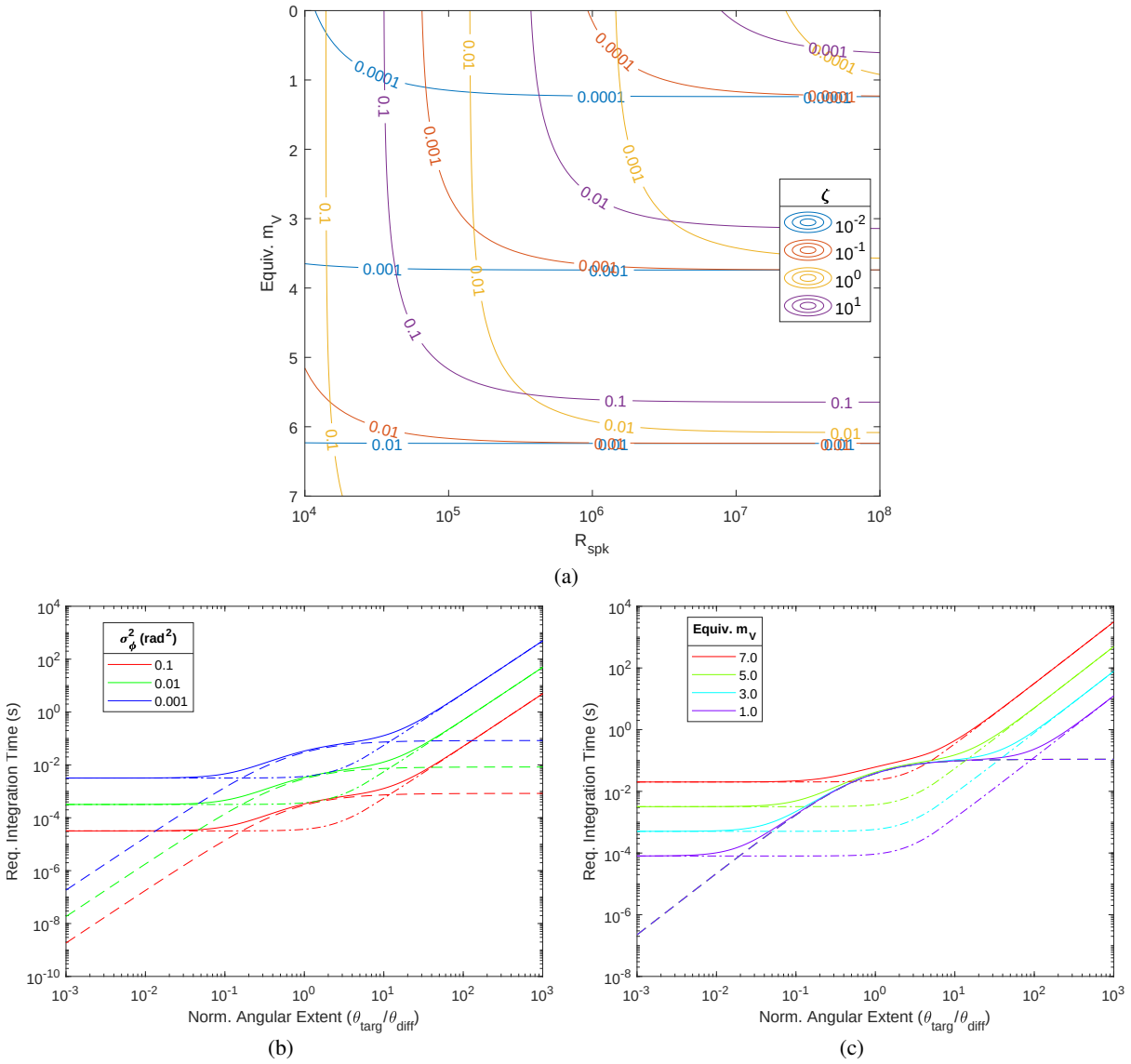

Figure 5: (a) Contour plot of required integration time in seconds required to reach $\sigma_\phi^2 = 1 \times 10^{-3}$ rad^2 (wavefront sensing MSE) in the presence of photon and speckle noise. Axes show varying target brightness in equivalent visible magnitude and rate of speckle realization update in realizations per second. Colors designate different target angular extent ζ. (b)-(c) Show reuired integration time for varying ζ assuming speckle evolution is driven by the movement of a target in a 1000 km orbit. Dashed lines show time required in the presence of only speckle noise, while dot-dash shows result for only photon noise. Solid lines show result in the presence of both. (b) Assumes a source with equivalent visual magnitude of 5.0 and a required σ_ϕ^2 in rad^2 as shown in the legend. (c) shows time required for σ_ϕ^2 of 0.001 rad^2 with target equivalent visual magnitude as shown in the legend.

Copyright © 2020 Advanced Maui Optical and Space Surveillance Technologies Conference (AMOS) – www.amostech.com

The plots and physical relationships presented in this work represent a simple method for the analysis of SHWFS in target-in-the-loop beam projection systems. Of particular interest are the results that photon noise adds in quadrature with speckle noise, and that speckle noise is dependent only on the normalized angular extent parameter $\theta_{ap}/\theta_{diff}$. Future systems with extremely large diameters will not be able to tolerate the focal anisoplanatism of laser guide-stars, so may be forced to rely on target reflected light. This work shows that such a sensing modality is feasible, and provides a useful resource for system architects.

ACKNOWLEDGMENTS

Many thanks to Ryan Allured and Jon Ashcom of MIT Lincoln Laboratory for helpful conversations, advice, and guidance in this work.
The authors acknowledge the MIT Lincoln Laboratory Supercomputing Center for providing high-performance computing resources that have contributed to the research results reported within this paper.

DISTRIBUTION STATEMENT A. Approved for public release. Distribution is unlimited.

This material is based upon work supported by the Under Secretary of Defense for Research and Engineering under Air Force Contract No. FA8702-15-D-0001. Any opinions, findings, conclusions or recommendations expressed in this material are those of the author(s) and do not necessarily reflect the views of the Under Secretary of Defense for Research and Engineering.

© 2020 Massachusetts Institute of Technology.

Delivered to the U.S. Government with Unlimited Rights, as defined in DFARS Part 252.227-7013 or 7014 (Feb 2014). Notwithstanding any copyright notice, U.S. Government rights in this work are defined by DFARS 252.227-7013 or DFARS 252.227-7014 as detailed above. Use of this work other than as specifically authorized by the U.S. Government may violate any copyrights that exist in this work.

REFERENCES

[1] C. R. Phipps et al. "Removing Orbital Debris with Lasers". In: *Advances in Space Research* 49.9 (May 2012), pp. 1283–1300. DOI: 10.1016/j.asr.2012.02.003.

[2] D. M. Cornwell. "NASA's Optical Communications Program for 2017 and Beyond". In: *2017 IEEE International Conference on Space Optical Systems and Applications (ICSOS)*. Nov. 2017, pp. 10–14. DOI: 10.1109/ICSOS.2017.8357203.

[3] P. Lubin. "A Roadmap to Interstellar Flight". In: *JBIS* 69 (Feb. 2016), pp. 40–72.

[4] P. Lubin et al. "Toward Directed Energy Planetary Defense". In: *Opt. Eng* 53.2 (Feb. 2014), p. 025103. DOI: 10.1117/1.OE.53.2.025103.

[5] J. W. Hardy. *Adaptive Optics for Astronomical Telescopes*. New York, NY: Oxford University Press, Inc., 1998.

[6] J. W. Goodman. *Speckle Phenomena in Optics*. Greenwood Village, CO: Roberts and Company Publishers, 2007.

[7] G. A. Tyler. "Accommodation of Speckle in Object-Based Phasing". In: *JOSA A* 29.5 (May 2012), pp. 722–733.

[8] M. A. Vorontsov and V. Kolosov. "Target-in-the-Loop Beam Control: Basic Considerations for Analysis and Wave-Front Sensing". In: *J. Opt. Soc. Am. A* 22.1 (Jan. 2005), p. 126. DOI: 10.1364/JOSAA.22.000126.

[9] A. S. Goncharov et al. "The Impact of Speckle on the Measurement of Eye Aberrations". In: *Journal of Modern Optics* 62.21 (Dec. 2015), pp. 1775–1780. DOI: 10.1080/09500340.2014.971895.

[10] M. A. Vorontsov, V. V. Kolosov, and E. Polnau. "Target-in-the-Loop Wavefront Sensing and Control with a Collett-Wolf Beacon: Speckle-Average Phase Conjugation". In: *Appl. Opt.* 48.1 (Jan. 2009), A13. DOI: 10.1364/AO.48.000A13.

[11] A. V. Larichev et al. "Measurement of Eye Aberrations in a Speckle Field". In: *Quantum Electron.* 31.12 (Dec. 2001), pp. 1108–1112. DOI: 10.1070/QE2001v031n12ABEH002105.

[12] A. A. Goloborodko et al. “Aberration Measurements in Speckle Field by Shack–Hartmann Wavefront Sensor”. In: *Opt. Eng* 55.12 (July 2016), p. 121710. DOI: 10.1117/1.OE.55.12.121710.

[13] R. J. Sasiela. *Electromagnetic Wave Propagation in Turbulence: Evaluation and Application of Mellin Transforms*. Second. SPIE Press, 2007.

[14] G. Rousset. “Wave-Front Sensors”. In: *Adaptive Optics in Astronomy*. Ed. by F. Roddier. Cambridge University, 1999, pp. 91–130.

[15] W. Southwell. “Wave-Front Estimation from Wave-Front Slope Measurements”. In: *J. Opt. Soc. Am.* 70.8 (Aug. 1980), p. 998. DOI: 10.1364/JOSA.70.000998.

[16] S. Thomas et al. “Comparison of Centroid Computation Algorithms in a Shack-Hartmann Sensor”. In: *Monthly Notices of the Royal Astronomical Society* 371.1 (Aug. 2006), pp. 323–336. DOI: 10.1111/j.1365-2966.2006.10661.x.

[17] J. W. Goodman. *Fourier Optics*. Third. Greenwood Village, CO: Roberts and Company Publishers, 2005.

[18] R. Soummer et al. “Fast Computation of Lyot-Style Coronagraph Propagation”. In: *Opt. Express* 15.24 (2007), p. 15935. DOI: 10.1364/OE.15.015935.

A. SHOT NOISE IN A SPECKLE FIELD

The probability distribution $p_H(H)$ of the number of photons H measured in each pixel is thus a compound distribution

$$p_H(H) = \int_0^\infty p_P(H|I)p_I(I)dI. \tag{A1}$$

Where $p_I(I)$ is the distribution of speckle intensity as shown in Eq. A3. The distribution for photon noise conditioned on intensity is given by

$$p_P(H|I) = \frac{I^H e^{-I}}{H!}. \tag{A2}$$

This is the probability mass function of measured photon count H, given by a Poisson distribution with mean I. The distribution $p_I(I)$ of speckle intensity is also well known. For speckle propagated through free space, the intensity at any point in the far field can be considered a sum of many independent complex phasors. This random walk in the complex plane results in an intensity with a negative exponential probability distribution

$$p_I(I) = \frac{1}{\langle I\rangle}\exp\Big(\frac{I}{\langle I\rangle}\Big). \tag{A3}$$

Where $\langle I\rangle$ is the ensemble average intensity over all realizations of the random speckle pattern. This is the same intensity which would be measured for an incoherently-illuminated target [17]. The instantaneous intensity at a point in the image plane evidently follows the same distribution for the case where $D_{corr} << D_{ap}$, as the image plane is a sum of many correlation areas in the pupil. Numerical experiments show this also to be true in the $D_{corr} > D_{ap}$ case, but are beyond the scope of this paper.

We are interested in the covariance between pixels, defined by $\mathrm{Cov}(H_i,H_j) = \langle H_i,H_j\rangle - \langle H_i\rangle\langle H_j\rangle$. Through direct summations over the distribution $p_H(H)$, we can find the moments of the distribution. We notice that the mean is simply the speckle-mean intensity as follows.

$$E_H[H] = \sum_{H=0}^{\infty}\int_0^\infty H\ p_P(H|I)\ p_I(I)\ dI \tag{A4}$$

$$= \int_0^\infty I\ p_I(I)\ dI \tag{A5}$$

$$= E_I[I] = \langle I\rangle \tag{A6}$$

And the expectation of the product is given by

$$\langle H_i,H_j\rangle = \sum_{H_i=0}^{\infty}\sum_{H_j=0}^{\infty}\int_0^\infty\int_0^\infty H_iH_j\ p_P(H_i,H_j|I_i,I_j)\ p_I(I_i,I_j)\ dI_i\ dI_j. \tag{A7}$$

Copyright © 2020 Advanced Maui Optical and Space Surveillance Technologies Conference (AMOS) – www.amostech.com

For $i = j$, we can calculate the second moment

$$\langle H_i, H_i \rangle = \langle H^2 \rangle = \sum_{H=0}^{\infty} \int_0^{\infty} H^2 \; p_P(H|I) \; p_I(I) \; dI \tag{A8}$$

$$= \int_0^{\infty} (I + I^2) p_I(I) \; dI \tag{A9}$$

$$= \langle I \rangle + \langle I^2 \rangle = \langle I \rangle + 2\langle I \rangle^2. \tag{A10}$$

Where in the last step we have used a well-known property of the negative exponential distribution. This leads to the conclusion that

$$\begin{aligned} \mathrm{Var}_H(H) &= \langle I \rangle + \langle I \rangle^2 \\ &= \mathrm{Var}_P(H|I = \langle I \rangle) + \mathrm{Var}_I(I). \end{aligned} \tag{A11}$$

Which is to say that the total variance in measured intensity is that due to speckle noise, plus that which would be expected of photon noise if the target was illuminated with incoherent light. For the case $i \neq j$ we use the knowledge that photon noise in neighboring pixels is independent, so the mutual distribution of pixel value conditioned on intensity is

$$p_P(H_i, H_j | I_i, I_j) = p_P(H_i|I_i) p_P(H_j|I_j). \tag{A12}$$

Plugging this into with Eq. A7, we find that $\langle H_i, H_j \rangle = \langle I_i, I_j \rangle$. Combining with Eq. A11, we find the general expressionf or covariance.

$$\mathrm{Cov}(H_{i,j}, H_{k,l}) = \delta_{i,k}\delta_{j,l}\mathrm{Var}_{ph}(H_{i,j}) + \mathrm{Cov}_{spk}(I_{i,j}, I_{k,l}) \tag{A13}$$

Where $\delta_{i,k}$ is the Kronecker delta. We see that the measured intensity covariance is made up of independent photon and speckle noise terms, so the centroiding variance is as well. (See Eq. 2.)

B. SHOT NOISE WITH A TOP-HAT PROFILE

For a fully-resolved, uniformly-illuminated, circular object, the intensity on the image plane can be represented as

$$P(x,y) = \frac{N_{ph}}{\pi R^2} \mathrm{circ}\left(\frac{\sqrt{x^2+y^2}}{R}\right). \tag{B1}$$

Where the total intensity is N_{ph} and the circle function is defined by

$$\mathrm{circ}(\rho) = \begin{cases} 1, & \text{if } \rho \leq 1 \\ 0, & \text{otherwise.} \end{cases} \tag{B2}$$

For the case of a well-resolved spot, the centroiding error due to photon noise as in Eq. 6 can be represented as an integral over a continuous domain:

$$\sigma_{ph}^2 = \frac{1}{N_{ph}^2} \int_{-w/2}^{w/2} \int_{-w/2}^{w/2} x^2 P(x,y) dx dy \tag{B3}$$

Substituting Eq. B1 and performing a change of variables, this becomes

$$\sigma_{circ}^2 = \frac{1}{N_{ph}\pi R^2} \int_0^{2\pi} \int_0^{R} (\rho\cos\theta)^2 \rho d\rho d\theta \tag{B4}$$

$$= \frac{1}{N_{ph}\pi R^2} \int_0^{2\pi} \cos^2\theta d\theta \int_0^{R} \rho^3 d\rho \tag{B5}$$

$$= \frac{1}{N_{ph}\pi R^2} \pi\left(\frac{R^4}{4}\right) = \frac{R^2}{4N_{ph}}. \tag{B6}$$

Copyright © 2020 Advanced Maui Optical and Space Surveillance Technologies Conference (AMOS) – www.amostech.com

If the spatial parameters x, y are assumed to be in units of diffraction angle λ/D_{ap}, then the radius R of the image takes the value

$$R = \frac{D_{targ}}{2z}\frac{D_{ap}}{\lambda} = \frac{1}{2}\frac{\theta_{targ}}{\theta_{diff}}. \tag{B7}$$

So the centroiding error is seen to be a function of the normalized target extent

$$\sigma^2_{circ} = \frac{1}{16N_{ph}}\left(\frac{\theta_{targ}}{\theta_{diff}}\right)^2. \tag{B8}$$

C. SPECKLE SLOPE STATISTICS

In the limit where, $\theta_{targ} << \theta_{diff}$ the effect of the speckle field is primarily that of a phase ramp across the SHWFS subaperture. The error in the wavefront slope measurement is therefore an offset due to the local slope of the speckle field. The derivative of the phase in a speckle field is given by [6] as

$$p(\phi_x) = \frac{\sqrt{d}}{2(1+d\phi_x^2)^{3/2}}. \tag{C1}$$

Where ϕ_x is the derivative of the phase along an arbitrary direction x, and d is a geometric factor related to the target geometry. For a circular object,

$$d = \frac{64\lambda^2 z^2}{\pi^3 D_{targ}^2} = \frac{64 D_{ap}^2}{\pi^3 \zeta^2}. \tag{C2}$$

The distribution is zero-mean, but its variance is indefinite. We can however truncate the distribution and calculate the variance by

$$\mathrm{Var}(\phi_x) = \int_{-L}^{L} \phi_x^2 p(\phi_x)\, d\phi_x = \frac{1}{d}[\sinh^{-1}(\sqrt{d}L) - \frac{dL}{\sqrt{d(dL^2+1)}}]. \tag{C3}$$

Limiting the phase slope to angles within the FOV of the subaperture, we can convert this angle to a phase slope and set the value of L as

$$L = \frac{w\lambda}{2D_{ap}}\frac{2\pi}{\lambda} = \frac{w\pi}{2D_{ap}}. \tag{C4}$$

Where w is the full FOV of the subaperture in units of λ/D_{ap}. If we assume that the value of ζ is large such that $\sqrt{d}L >> 1$, we can simplify Eq. C3 as

$$\mathrm{Var}(\phi_x) = \frac{1}{d}[\log(\sqrt{\sqrt{d}L+1} + \sqrt{d}L) - \frac{dL}{\sqrt{d(dL^2+1)}}] \tag{C5}$$

$$= \frac{1}{d}[\log(2\sqrt{d}L) - 1]. \tag{C6}$$

We can now substitute the values of d and L and convert to units of angle, giving an expression for centroiding error due to speckle that is applicable in the case of an unresolved target.

$$\sigma^2_{spk} = \left(\frac{\lambda}{D_{ap}}\right)^2 \frac{\pi\zeta^2}{256}\left[\log\left(\frac{16w}{\sqrt{\pi}\zeta}\right) - 1\right] \tag{C7}$$

We notice that the value of the logarithmic term changes little with ζ, compared with the ζ^2 term, so σ_{spk} is approximately proportional to the normalized angular extent ζ of the target.

D. AVERAGING OF SPECKLE REALIZATIONS

In the case of an average SHWFS image over multiple independent speckle realizations, we begin with the equation for centroiding noise due to speckle.

$$\sigma^2_{\alpha,spk} = \frac{1}{N_{ph}^2}\sum_{i,j}\sum_{k,l} x_{i,j}x_{k,l}\mathrm{Cov}(I_{i,j}, I_{k,l}). \tag{D1}$$

Copyright © 2020 Advanced Maui Optical and Space Surveillance Technologies Conference (AMOS) – www.amostech.com

We replace the intensity at each pixel by the average over speckle realizations,

$$I_{i,j}^{av} = \frac{1}{M} \sum_{m=1}^{M} I_{i,j}^{(m)}. \tag{D2}$$

We note that the speckle realizations being averaged are uncorrelated, and each $I_{i,j}^{(m)}$ is distributed identically as $I_{i,j}$. Without directly addressing the correlation between pixel values, we can state

$$\mathrm{Cov}(I_{i,j}^{av}, I_{k,l}^{av}) = \frac{1}{M} \mathrm{Cov}(I_{i,j}, I_{k,l}). \tag{D3}$$

And therefore that the variance of the speckle noise decreases as the number of independent realizations averaged.

$$(\sigma_{\alpha,spk}^{av})^2 = \frac{1}{M} \sigma_{\alpha,spk}^2 \tag{D4}$$

Copyright © 2020 Advanced Maui Optical and Space Surveillance Technologies Conference (AMOS) – www.amostech.com